Title: Anormal thermal history effect on the structural dynamics of probucol infiltrated into porous alumina

Author: Agnieszka Talik, Magdalena Tarnacka, Aldona Minecka, Barbara Hachuła, Joanna Grelska, Karolina Jurkiewicz, Kamil Kamiński, Marian Paluch, Ewa Kamińska

Citation style: Talik Agnieszka, Tarnacka Magdalena, Minecka Aldona, Hachuła Barbara, Grelska Joanna, Jurkiewicz Karolina, Kamiński Kamil, Paluch Marian, Kamińska Ewa. (2021). Anormal thermal history effect on the structural dynamics of probucol infiltrated into porous alumina. "Journal of Physical Chemistry C" (Vol. 125, iss. 7 (2021), s. 3901-3912), doi 10.1021/acs.jpcc.0c10560

THE JOURNAL OF PHYSICAL CHEMISTRY C
A JOURNAL OF THE AMERICAN CHEMICAL SOCIETY

pubs.acs.org/JPCC

Article

Anormal Thermal History Effect on the Structural Dynamics of Probucol Infiltrated into Porous Alumina

Agnieszka Talik,* Magdalena Tarnacka,* Aldona Minecka, Barbara Hachuła, Joanna Grelska, Karolina Jurkiewicz, Kamil Kaminski, Marian Paluch, and Ewa Kaminska

Cite This: J. Phys. Chem. C 2021, 125, 3901−3912

Read Online

ACCESS | Metrics & More | Article Recommendations | Supporting Information

ABSTRACT: Herein, broadband dielectric (BDS) and Fourier transform infrared spectroscopy (FTIR), together with differential scanning calorimetry (DSC) and X-ray diffraction (XRD), were applied to study the molecular dynamics, molecular interactions as well as physical stability of an amorphous Active Pharmaceutical Ingredient (API)—probucol (PRO)—infiltrated into anodic aluminum oxide (AAO) membranes of pore size, $d \sim 10-160$ nm. Interestingly, the behavior of examined substance strongly depends on the applied thermal protocol. Remarkably, for the first time, we observed that the structural dynamics of the slowly cooled PRO under confinement is significantly enhanced when compared to that of the quenched material. This unusual behavior was interpreted as a result of surface-induced effects (including the formation of well-resolved interfacial H-bonded layer and adsorption−desorption processes near the interface) that are magnified by the extremely high sensitivity to density fluctuation of studied PRO, reflected in the enormous pressure coefficient of the glass transition temperature $dT_g/dp = 427$ K/GPa. In fact, FTIR investigations revealed that PRO tends to self-associate under confinement and forms a strongly bonded interfacial layer, which controls the variation in the structural dynamics of core molecules. Finally, we observed that the tendency to crystallize of confined API is reduced with respect to the bulk, even though the critical size of PRO nuclei ($r_c \sim 3$ nm) is significantly lower than the smallest examined pore size. Nevertheless, after few weeks of storage, the investigated substance crystallized in larger pores, while it remained stable in the nanochannels of $d = 10$ nm. A combination of XRD and DSC measurements indicated that the infiltrated PRO forms two polymorphs, the stable form I (dominating in bulk) and unstable form II (prevailing under confinement). That means that porous matrices might be used to obtain and maintain prolonged stability of unstable polymorphic forms of API.

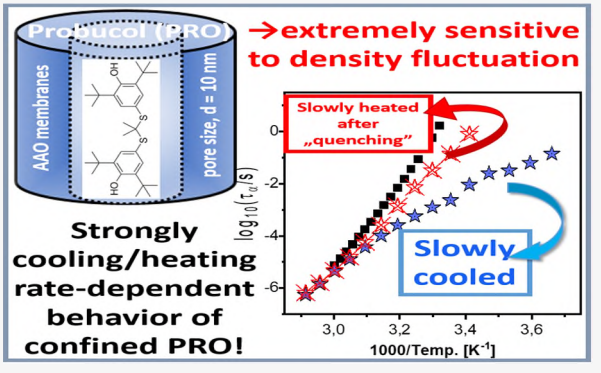

1. INTRODUCTION

Almost 40% of available and commercially used Active Pharmaceutical Ingredients (APIs), and the majority of the new API candidates are poorly water-soluble drugs (classified as the second and fourth class of the Biopharmaceutics Classification System, BCS). Therefore, a great effort has been put into increasing their solubility and bioavailability, allowing application of lower therapeutic doses and reducing toxic side effects.[1] In fact, to date, different strategies have been considered and developed to enhance these pharmaceutically important parameters, including (i) the use of pro-drugs,[2] (ii) salt formation (tartrate, succinate, mesylate, nitrate, hydrochloric),[3,4] (iii) micronization,[5−7] (iv) cocrystallization,[8,9] (v) formation of solid dispersions with soluble polymers (or saccharides),[10,11] and (vi) amorphization.[12] In recent years, the last approach attracted increasing attention of the scientists and industry since the amorphous APIs are generally characterized by higher solubility (due to the lower energy barrier required to dissolve the molecule[13,14]) and, consequently, bioavailability with respect to their crystalline counterparts. However, it should be pointed out that the commercial use of pharmaceuticals prepared in the amorphous form is limited, mainly due to their physical instability, which is reflected in a strong tendency to recrystallization. As a consequence, the advantages given by the amorphous state are lost during storage.[12] The most convenient way to stabilize amorphous APIs is mixing them with various excipients,[15] i.e., modified mono-, di, and oligosaccharides,[10,16−20] polymers,[21−25] and amino acids.[26−28] In such case, so-called coamorphous systems of enhanced physical stability are created. The other unique alternative to affect and stabilize disordered pharmaceuticals is infiltration them into porous templates made of inert, biocompatible, nontoxic materials

Received: November 24, 2020
Revised: January 30, 2021
Published: February 16, 2021

https://dx.doi.org/10.1021/acs.jpcc.0c10560
J. Phys. Chem. C 2021, 125, 3901−3912

composed of pores of varying geometry, morphology, and size (d), considered as 2D confinement.[15]

Systematic studies on various highly crystallizing active substances, such as, i.e., menthol,[29] ezetimibe,[33] naproxen,[30] and ibuprofen[31,32] at the nanoscale successfully demonstrated that when the size of the nanochannel is smaller than the diameter of the critical radius of nucleation, r_c, the infiltrated materials reveal no tendency to crystallization and remain amorphous upon long-term storage.[33,34] In this context, one can briefly mention that the bulk naproxen and menthol cannot be supercooled below their glass transition temperature (T_g), avoiding crystallization, irrespective of the applied cooling rate.[35] A similar situation was observed in the case of water. However, after the infiltration of water into pores of nanometrical diameter, d = 2.6 nm, which is smaller than its r_c, the crystallization was strongly suppressed. The other benefit of investigations on confined water is a unique opportunity to calculate approximately its T_g and verify the fragile to strong transition in this system, both hotly debated problems in the literature. It is also worth mentioning the studies by Floudas group, which revealed the change in character of the nucleation that can be tuned by the pore diameter.[36] The authors demonstrated a transition from the heterogeneous nucleation of hexagonal ice (I_h) to the homogeneous nucleation of predominantly cubic ice (I_c) in AAO membranes characterized by different pore sizes.[37,38]

In the literature, one can also find a lot of reports concerning the studies on the crystallization kinetics in liquids/APIs infiltrated in pores.[34,43] It was shown that the rate of crystallization as well as the maximum in the temperature dependence of the constant rates of this process change in pores of varying diameter and surface functionality. Moreover, it was noted that the melting temperature of the formed crystals decreases with pore size.[34] In fact, the modeling of this relationship using the Gibbs−Thomson equation[39,40] allows calculating the interfacial free energy between crystal and liquid states, σ_{cl}, which cannot be obtained from any other currently available experimental methods. One can add that this parameter is a key quantity to evaluate the critical radius of nuclei and predict the energy barrier for the nucleation process. It is also worth stressing that the application of nanoporous templates of varying morphologies can be very useful to obtain new polymorphic forms of APIs, which are often characterized by different physicochemical properties. Such a scenario was noted for salol incorporated into AAO templates, where dependent on the pore size, stable (orthorhombic crystal) or unstable (monoclinic form) polymorphic forms of this API were obtained in larger and smaller pores, respectively.[43] As mentioned above, a similar finding was also reported for water, where a clear change in the crystal lattice from the hexagonal ice into the cubic one, due to increased interactions with the pore walls, was observed.[35,36] Moreover, it is worth adding that the incorporation of glycine into pores allowed one to enhance the stability of the nonstable β-polymorph inside nanoporous host matrices with respect to the bulk state of this amino acid, for which a more thermodynamically stable α-form is preferred.[41] Additionally, the crystallization kinetics changes have also been reported for acetaminophen drug confined into controlled porous glasses (CPGs), where three different crystalline forms were investigated, dependent on the applied pore diameter.[42] Therefore, it seems that by using porous templates of appropriate pore size, one can increase the control over both the overall crystallization process and the growth of new polymorphs.[43]

Simultaneously to studying the crystallization of materials infiltrated into porous templates, a great effort has been made to understand the variation in molecular dynamics of such systems, which, aside from the thermodynamic driving force, is one of the most important factors that control the rate of nucleus formation and growth of crystals. It was found that, for most confined liquids, a clear deviation of structural/segmental and local relaxation times from the bulk behavior is observed.[34,33] In the literature, this finding is usually discussed in the context of competition between the finite-size effects and free volume or surface interactions.[31,32,44−47] However, the contribution of these factors remains a challenge and requires further investigations.

In this paper, we examined the molecular dynamics of probucol (PRO) incorporated into AAO membranes of varying pore diameters, $d \sim 10-160$ nm, by means of different experimental techniques, broadband dielectric (BDS) and Fourier transform infrared (FTIR) spectroscopy, as well as differential scanning calorimetry (DSC). Additionally, the structure of bulk and confined PRO was examined using X-ray diffraction (XRD). This type of investigations seems to be important considering previous report demonstrating the enhancement in dissolution rate and antioxidant properties of PRO confined in mesoporous silica with respect to the bulk crystalline material.[48] It is also worth stressing that recent studies have indicated that this API is characterized by an extremely high (one of the highest reported to date) pressure coefficient of the glass transition temperature, dT_g/dp = 427 K/GPa,[49] which quantifies the sensitivity of the structural relaxation dynamics to the density fluctuation. Therefore, it seems to be a perfect candidate to probe the impact of surface interactions with pore walls on the molecular mobility for the samples confined into porous templates.

2. EXPERIMENTAL SECTION

2.1. Materials. Probucol, 4,4′-[propane-2,2-diylbis(thio)]-bis(2,6-di-*tert*-butylphenol), $C_{31}H_{48}O_2S_2$, with M_w = 516.84 g/mol, and purity >98%, was supplied by TCI Europe. The nanoporous alumina oxide membranes used in this study (supplied from InRedox) are composed of uniaxial channels (open from both sides) with well-defined pore diameter, $d \sim$ 160, 120, 80, 20, 10 ± 2 nm, thickness ∼50 ± 2 μm, and porosity ∼12 ± 2%. Details concerning the pore density, distribution, etc., can be found on the webpage of the producer.[50]

2.2. Sample Preparation. The applied AAO membranes were dried in an oven at T = 423 K under a vacuum (10^{-2} bar) for at least t = 24 h to remove any volatile impurities from the nanochannels. After cooling, probucol was placed on the top of the AAO templates. Then, the whole system was kept at T = 398 K under vacuum for at least 6 h, which allows the liquid to flow inside the nanopores by capillary forces (chemical stability of PRO has been confirmed by nuclear magnetic resonance (NMR) studies). The membranes were weighted before and after infiltration. The complete filling was obtained if the mass of the membrane ceased to increase. After completing the infiltration process, the surface of the AAO membrane was heated to T = 398 K and dried at atmospheric pressure to remove the excess sample on the surface by a metal blade and a paper towel.

https://dx.doi.org/10.1021/acs.jpcc.0c10560
J. Phys. Chem. C 2021, 125, 3901−3912

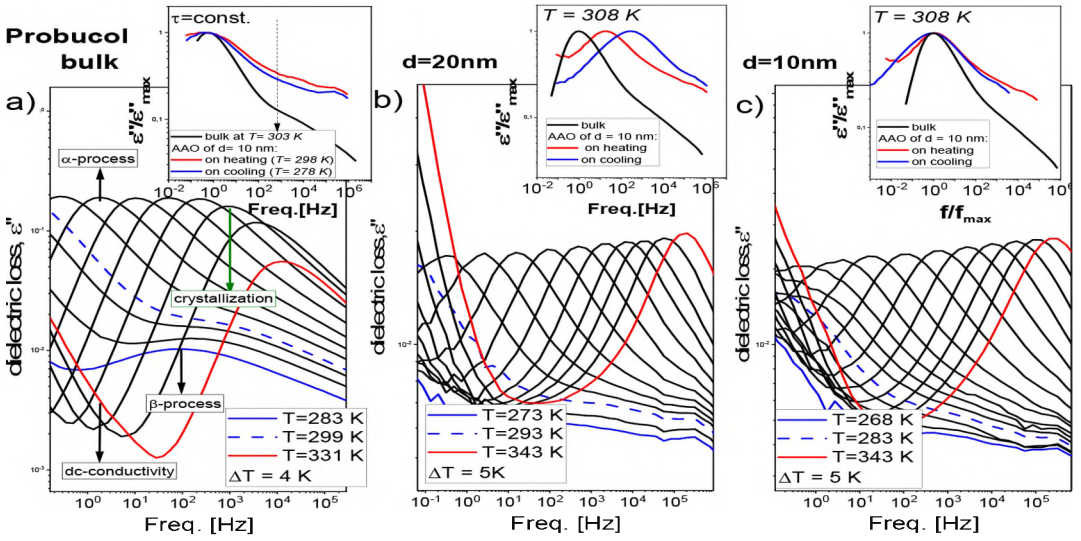

Figure 1. Dielectric loss spectra of bulk probucol (PRO) (a) and confined into AAO templates of d = 20 nm (b) and d = 10 nm (c). As the inset in panel a, the superposed dielectric spectra measured in the vicinity of T_g were presented to highlight the presence of the β-process. Additionally, in the insets to panels b and c, the normalized loss spectra collected for bulk PRO and API infiltrated into AAO pores of d = 10 nm at T = 308 K (b), which further were shifted horizontally to superpose at the maximum (c), are shown. Note that the data for the bulk sample were taken from ref 49.

2.3. Methods. *2.3.1. Broadband Dielectric Spectroscopy (BDS).* Isobaric measurements of the complex dielectric permittivity $\varepsilon^*(\omega) = \varepsilon'(\omega) - i\varepsilon''(\omega)$ were carried out using the Novocontrol Alpha dielectric spectrometer over the frequency range from 10^{-1} to 10^6 Hz at ambient pressure. The temperature uncertainty controlled by a Quatro Cryosystem using a nitrogen gas cryostat was better than 0.1 K. The data for bulk substance have been taken from ref 49. The sample was placed in the capacitor with 20 mm of diameter and 0.1 mm distance between the plates. Examined samples were prepared by the vitrification method at ambient pressure. The bulk PRO was cooled from above the melting temperature deeply below T_g and then measured on heating, in the temperature range from 223 to 331 K. For details, please see ref 49.

For confined systems, dielectric measurements were carried out on AAO membranes filled with PRO and placed in a capacitor with 10 mm of diameter (membrane thickness: 0.05 mm).[51,52] Nevertheless, the confined sample is a heterogeneous dielectric consisting of a matrix and an investigated compound. Because the applied electric field is parallel to the long pore axes, the equivalent circuit consists of two capacitors in parallel composed of $\varepsilon^*_{compound}$ and ε^*_{AAO}. Thus, the measured total impedance is related to the individual values through $1/Z^*_c = 1/Z^*_{compound} + 1/Z^*_{AAO}$, where the contribution of the matrix is marginal. The measured dielectric spectra were corrected according to the method presented in ref 53.

Note that during dielectric measurements of the examined confined systems, we applied two different temperature protocols: (i) "slow cooling from the room temperature (RT)," where the samples have been slowly cooled (cooling rate dT/dt tends to 0 K/min) from T = 298 K below T_g; and (ii) "slow heating of the quenched samples," where the samples have been cooled deeply below T_g (with the cooling rate 50 K/min) and then slowly heated (heating rate dT/dt tends to 0 K/min) from the glassy state into the higher temperatures.

2.3.2. Differential Scanning Calorimetry (DSC). Calorimetric measurements were carried out using a Mettler−Toledo DSC apparatus (Mettler-Toledo International, Inc., Greifensee, Switzerland) equipped with a liquid nitrogen cooling accessory and an HSS8 ceramic sensor. Temperature and enthalpy calibrations were investigated using indium and zinc standards, and the heat capacity, C_p, calibration was performed using a sapphire disc. Measurements of confined systems were carried out by crushed filled membranes to fix the measurement alumina crucibles. After placing crushed templates in the crucibles, they were sealed and measured over a wide temperature range with different cooling rates, 2, 10, and 20 K/min, and a heating rate equal to 10 K/min.

2.3.3. Fourier Transform Infrared Spectroscopy (FTIR). FTIR measurements were performed on a Thermo Scientific Nicolet iS50 spectrometer equipped with a Linkam THMS 600 (Linkam Scientific Instruments Ltd., Surrey, U.K.) heating/cooling stage. FTIR spectra were collected at a spectral resolution of 4 cm^{-1} with 32 coadding scans in the frequency range of 4000−1300 cm^{-1}. The limited measurement range resulted from the absorption of AAO membranes. The temperature stabilization accuracy was equal to ±0.1 K. In the first rate-dependent experiment, the confined PRO within AAO membranes was heated to 343 K at a heating rate of 10 K min^{-1}, held for 5 min and then cooled to 308 K at the different cooling rates (5, 10, 15, 20, and 30 K min^{-1}). For the second time-dependent experiment, the melted samples were cooled to 308 K with a constant 20 K min^{-1} cooling rate. The time-dependent IR spectra were collected at 1 min intervals at T = 308 K for 30 min.

2.3.4. X-ray Diffraction (XRD). XRD measurements were performed on a Rigaku-Denki S/MAX RAPID II-R diffractometer equipped with an image plate detector, a rotating Ag anode and an incident beam (002) graphite monochromator (wavelength of incident beam λ = 0.56 Å). Samples of bulk PRO (measured as received from TCI Europe) and PRO infiltrated into AAO membrane of d = 80 nm were ground in a mortar, packed into glass-capillaries of 1.5 mm diameter and measured at T = 293 K. Additionally, pure AAO membrane was probed. The sample of PRO within the AAO template was measured just after 1 and 50 days of storage under normal

https://dx.doi.org/10.1021/acs.jpcc.0c10560
J. Phys. Chem. C 2021, 125, 3901−3912

conditions. The diffraction data were collected as two-dimensional patterns and converted into a one-dimensional function of scattering intensity versus the scattering angle 2θ. The final results show the diffractograms with subtracted background from an empty capillary.

3. RESULTS AND DISCUSSION

Dielectric loss spectra ($\varepsilon''(\omega)$) obtained for the bulk PRO and the API confined into AAO membranes of different pore sizes (d = 10 nm and d = 20 nm) are shown in Figure 1. The spectra of PRO infiltrated into alumina templates of higher pore diameters (d = 80 nm and d = 120 nm) are presented in Figure S1 in the Supporting Information. As shown, the measured spectra revealed the presence of dc-conductivity, responsible for the charge transport, a well-resolved structural (α) relaxation process, related to the cooperative motions of molecules and responsible for the glass transition, as well as the secondary Johari–Goldstein (JG) β-process, having intermolecular character and originating from local motions of the whole molecules.[49,54] It is important to note that this universal secondary mobility is well-observed for both bulk and confined PRO (the inset of Figure 1a), which is not always the case, especially in spatially restricted systems. Moreover, the data presented in Figure 1a reveal a systematic drop of the amplitude of α-relaxation process of bulk API measured above T > 320 K due to the ongoing crystallization.[49] On the other hand, for the infiltrated PRO, no crystallization can be seen upon the increasing temperature; see parts b and c of Figure 1. This implies the increased physical stability (lower crystallization ability) of supercooled and glassy PRO under confinement when compared to its bulk counterpart. Note that this issue will be discussed in detail in the last section of this paper.

Moreover, as illustrated in the inset to Figure 1c, a significant broadening of the α-relaxation for the confined samples with respect to the bulk is observed. It is worth recalling that such behavior commonly discussed in the context of increasing heterogeneity of the relaxation dynamics or the strength of interactions between molecules and pore walls is a common feature for substances infiltrated into porous templates.[55] This finding agrees with earlier reports for polypropylene glycol (PPG) or polyisoprene (PI) incorporated into silica and alumina templates.[56,57] Additionally, it should be mentioned that for the confined substances, we did not detect any interfacial process, reflecting the reorientational motions of adsorbed molecules. In this context, one can be remind that for many glass formers, especially those interacting with the matrix, the existence of such mobility is reported.[58−61,46]

Since recent studies on various low- and high- molecular weight glass formers infiltrated into AAO templates have indicated that the structural/segmental dynamics strongly depends on the thermal history of the confined sample,[62−64] we decided to explore this effect on spatially restricted PRO—a compound that is characterized by one of the highest pressure coefficient of the glass transition temperature, dT_g/dp = 427 K/GPa. For that purpose, dielectric measurements on the confined API were performed using two different temperature protocols described in detail in the Experimental Section. At first glance, any significant differences between samples measured at either slow cooling or heating were detected. However, when we compared dielectric spectra of bulk sample and API confined in pores of d = 10 nm, measured at the same temperature (T = 308 K), we noted a major variation in dynamical properties (shape and relaxation time) of the structural process for both systems, see inset to Figure 1b. Remarkably, the spectra of confined substance measured upon various experimental protocols differed significantly between each other. As shown, the α-relaxation peak recorded upon slow cooling is clearly shifted toward higher frequencies with respect to that obtained for the quenched API. It should be mentioned that all experiments reported to date have revealed opposite effects, i.e., very fast (quenched) systems were characterized by enhanced dynamics when approaching the T_g.[29−32,34]

To quantify the observed extraordinary differences between slowly cooled and quenched samples, we further analyzed the temperature dependences of structural relaxation times, τ_α. For that purpose, the measured dielectric loss spectra of the examined PRO systems, recorded upon both thermal protocols at $T > T_g$, have been analyzed using the Havriliak–Negami (HN) function with the conductivity term:[65]

$$\varepsilon(\bar{\omega})'' = \frac{\sigma_{dc}}{\varepsilon_0 \bar{\omega}} + \left(\frac{\Delta\varepsilon}{[1 + (i\bar{\omega}\tau_{HN})^{\alpha_{HN}}]^{\beta_{HN}}} \right) \quad (1)$$

Here α_{HN} and β_{HN} are shape parameters representing the symmetric and asymmetric broadening of given relaxation peaks, τ_{HN} is the HN relaxation time, ε_0 is the vacuum permittivity, $\Delta\varepsilon$ is the dielectric relaxation strength, and $\bar{\omega}$ is an angular frequency ($\bar{\omega} = 2\pi f$). Then, using the procedure described in ref 66, τ_α values have been obtained from τ_{HN}. The temperature dependences of τ_α estimated for all investigated samples, both bulk and confined, measured on slow cooling and heating, are presented in Figure 2. As can be seen, the relaxation times remain bulk-like at high temperatures

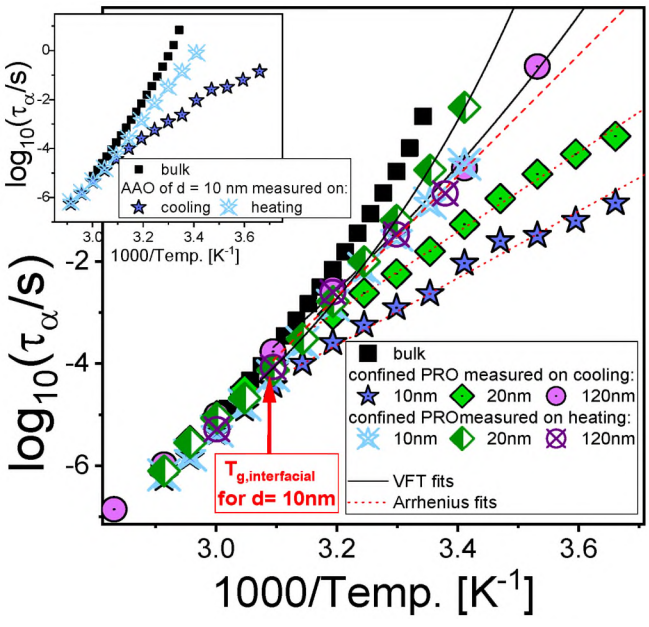

Figure 2. Temperature dependences of α-relaxation times for bulk PRO and API confined into AAO templates of various pore sizes. Black solid and red dashed lines are the best fits using VFT and Arrhenius equations, respectively. Inset: $\tau_\alpha(T)$-dependences obtained for PRO infiltrated into AAO membranes of d = 10 nm measured using two different protocols. Note that $\tau_\alpha(T)$-dependences determined for PRO within AAO templates of d = 80 nm are presented in Figure S2.

https://dx.doi.org/10.1021/acs.jpcc.0c10560
J. Phys. Chem. C 2021, 125, 3901−3912

Table 1. Values of T_g Estimated from Dielectric and Calorimetric Measurements for Bulk and Confined Samples Subjected to Different Thermal Treatments with Measurement Error ±2 K[a]

	BDS measurements				DSC measurements	
	slow cooling		slow heating		heating rate 10 K/min	
sample	$T_{g,interfacial}$ [K]	$T_{g,core}$ [K] for τ_α = 100 s	$T_{g,interfacial}$ [K]	$T_{g,core}$ [K] for τ_α = 100 s	$T_{g,interfacial}$ [K]	$T_{g,core}$ [K]
bulk		294		294		299
			PRO confined within AAO templates			
d = 80 nm	313	270	323	289	322	309
d = 20 nm	318	261	323	289	314	290
d = 10 nm	328	248	323	280	316	290

[a]Note that T_gs from calorimetric measurements were determined from the midpoint of the observed heat capacity jumps.

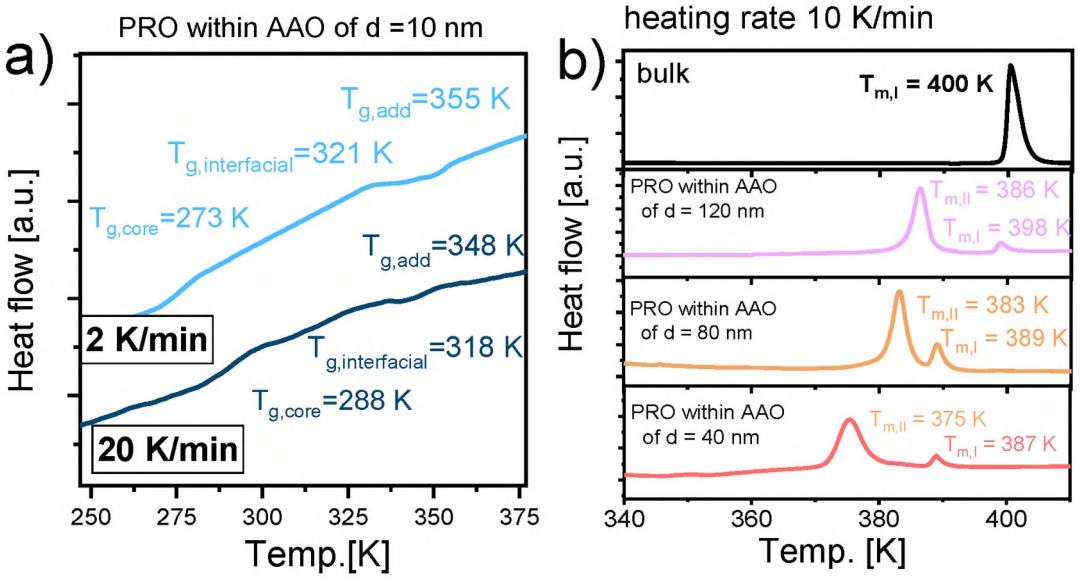

Figure 3. (a) DSC thermograms collected for PRO infiltrated into AAO templates of d = 10 nm measured at two different cooling rates, 2 and 20 K/min, with the following 10 K/min heating rate. (b) DSC thermograms of the crystalline bulk sample and PRO infiltrated into AAO membranes of various pore size (d = 40−120 nm), measured on heating with rate 10 K/min from RT well above the melting temperature of bulk API.

and deviate at some specific conditions labeled as $T_{g,interfacial}$. One can recall that this deviation occurring at $T_{g,interfacial}$ has been rationalized in terms of, i.e., the limited length scale of dynamic cooperativity of molecular motions,[67,68] or the vitrification of molecules strongly interacting with the interface (the interfacial layer).[62] Although the results obtained previously for glycerol infiltrated in metal−organic frameworks (MOF) supported the first hypothesis,[69,70] there are many reports, also coming from our group, confirming the latter explanation that was validated based on the combined dielectric and calorimetric investigations. Note that the data collected for various glass formers infiltrated into AAO templates of different d revealed that the deviation of $\tau_\alpha(T)$-dependences occurring at $T_{g,interfacial}$ corresponds well with the calorimetric high glass transition temperature recorded in thermograms. Simultaneously, the lower glass transition temperature is consistent (within a few kelvin) with the one calculated from $\tau_\alpha(T)$-dependences at temperature, at which τ_α = 100 s. These findings are in fair agreement with the very simple two-layer[60] (or shell−core) model describing the heterogeneity of the liquids confined in pores. In view of this approach, due to the various distance from the interface, there are at least two fractions of molecules within infiltrated materials: (i) those located in the center of porous nanochannels ("core") and (ii) those attached to the interface ("interfacial"), both characterized by different mobility and consequently T_g.[60] It should be pointed out that the comprehensive calorimetric measurements performed for the confined PRO have clearly shown two endothermic heat capacity jumps related to the glass transitions of interfacial, $T_{g,interfacial}$, and core, $T_{g,core}$, molecules (Figure S4). As observed, the values of $T_{g,interfacial}$ determined from DSC studies are in agreement with the temperatures, at which the deviation of $\tau_\alpha(T)$-dependences for infiltrated samples occur; see Table 1 and Figure 2. Therefore, herein, we assigned the vitrification of the interfacial layer as the origin of the variation of $\tau_\alpha(T)$ upon decreasing temperature.

Interestingly, as presented in Figure 2, the characteristic departure of τ_α from the bulk-like behavior can be noted for all examined infiltrated PRO independently to the applied thermal protocol. However, with decreasing temperature below $T_{g,interfacial}$, a significant difference in the slope of τ_α(T)-dependences between quenched and slowly cooled samples is observed. Remarkably, τ_α(T)-dependences of quenched materials are significantly steeper than the ones measured on slow cooling from RT, see the inset in Figure 2 and Figure S3. Consequently, the $T_{g,core}$ (related to the vitrification of core molecules) values of quenched samples are much higher with respect to those estimated for the slowly cooled API, whereas $T_{g,interfacial}$ (marked in Figure 2), reaches comparable values

https://dx.doi.org/10.1021/acs.jpcc.0c10560
J. Phys. Chem. C 2021, 125, 3901−3912

independent of the applied experimental protocol. For details concerning the determination of $T_{g,interfacial}$ and $T_{g,core}$, please see the Supporting Infomation. Note that the values of T_gs estimated from BDS measurements performed on the quenched samples were in good agreement with those determined from calorimetric measurements performed at a heating rate of 10 K/min; see Table 1.

We would like to highlight that, as mentioned above, the variation of the structural dynamics of confined PRO, where the slowly cooled sample is characterized by the enhanced dynamics when approaching $T_{g,core}$, is unexpected. One can add that the literature data for other glass formers confined at the nanoscale, i.e., for triphenyl phosphite (TPP),[62] PPG[57] and poly(methylphenylsiloxane) (PMPS),[71] show a different behavior. As reported, the slow cooling of infiltrated material results in more homogeneous dynamics and denser material with a higher $T_{g,core}$, whereas the quenching leads to a larger anisotropy and lower $T_{g,core}$. The differences between applied experimental protocols were assigned to the variation in density packing at the interface. It was assumed that in the former case, the infiltrated molecules have enough time for the local rearrangements and density equilibration (as well as the kinetic mass exchange between interface-core fractions). On the other hand, the rapid cooling freezes the local conformation of molecules under confinement, which cannot evolve upon the measurements.

To confirm the quite unusual behavior of the confined PRO observed upon dielectric studies, we carried out additional calorimetric measurements on infiltrated API, applying two different cooling rates (2 and 20 K/min) followed by a 10 K/min heating rate. The purpose of these experiments was to see how the thermal history affects the glass transition temperature (and thus, indirectly, the molecular dynamics) of confined systems. DSC thermograms of PRO infiltrated into AAO templates of d = 10 nm are shown in Figure 3a. Note that in this experiment, the investigated system was molten and then cooled with cooling rates, either 2 or 20 K/min, followed in both cases by a 10 K/min heating rate. The existence of the two T_gs can be confirmed by additional data treatment relying on the temperature derivative representation of specific heat capacity jumps, where two maxima peaks can be easily observed; please see Figure S5a. Interestingly, one can observe that the lowest T_g related to the vitrification of core molecules changes significantly with the experimental protocol, where $T_{g,core}$= 273 K and $T_{g,core}$= 288 K for cooling rates of 2 and 20 K/min, respectively. At this point, we would like to emphasize two issues. First, the variation of $T_{g,core}$ with the heating rate is significantly higher than the one usually observed in calorimetric measurements (note that it normally reaches $\Delta T_g \sim 5-6$ K, not $\Delta T_g \sim 15$ K as reported herein). Second, this behavior confirms the strong variation in $T_{g,core}$ determined from the analysis of dielectric data obtained for the confined PRO subjected to different thermal treatments, where the values of this temperature for the quenched samples were much higher than those estimated for the slowly cooled materials.

Additionally, it is worth pointing out that DSC thermograms of PRO infiltrated into AAO templates of d = 10 nm revealed, remarkably, the presence of the third endothermic heat capacity jump in the temperature range T > 320 K. Note that also in the case of the temperature derivative representation of DSC curved obtained for PRO confined within AAO templates of d = 10 nm, we can observe three maxima confirming the occurrence of an additional third glass transition temperature, see Figure S5b. One can add that this endothermic event changes accordingly to the applied heating rate; therefore, we considered it as a "normal" glass transition and not as an experimental artifact. This finding indicates the occurring of an additional third glass transition temperature of unknown origin (labeled as $T_{g,add}$). In this context, one can recall some earlier works on poly(methyl methacrylate) (PMMA),[72] PPG,[63] and PMPS[71] confined within AAO porous templates, reporting the existence of the third T_g, located between $T_{g,core}$ and $T_{g,interfacial}$ upon different heating/cooling rates due to the formation of the intermediate layer between the adsorbed and core molecules.[72] However, in our case, the additional $T_{g,\ add}$ is located far above $T_{g,interfacial}$, suggesting a different origin of this anomalous glass transition temperature. In fact, taking into account that the mobility of molecules under confinement reduces with a decreasing distance from the substrate/matrix interface, one can assume that the detected third heat capacity jump of unknown origin can be correlated to the response of, i.e., the molecules irreversible adsorbed on the pore walls. Alternatively, it might be due to some phase transition related to the change in the materials' wettability upon temperature decrease. However, at the moment, it is very difficult to verify which hypothesis is correct.

All the data reported and discussed above indicated rather peculiar behavior of PRO infiltrated into the porous matrix. Thus, the question arises, what is the origin of the observed anomalous structural dynamics of the confined API? Is it related to the variation in the density packing as previously reported in the literature?[53,73] Or rather with the formation of an irreversibly adsorbed layer (IAL) at the interface? One can recall that many factors are considered to affect soft matter's behavior spatially restricted to the nanoscale, including, i.e., finite size,[47] free volume,[74] and negative pressure.[59] However, the majority of recent papers devoted to this issue highlighted, in fact, the key role of surface effects on the dynamics of those materials.[53,59,75] Herein, we would also like to discuss the observed quite unusual behavior of incorporated PRO in terms of surface effects. We suppose that upon slow cooling, the infiltrated API molecules have more time to the density equilibration. Alternatively (or even additionally), the variation within the interface might include both adsorption−desorption processes at the interface and the exchange between core and interfacial molecules. Consequently, a well-resolved interfacial layer (or even IAL) might be formed. The dynamical and static properties of adsorbed molecules or eventual their vitrification further affect the behavior of confined PRO. In contrast, in the case of quenched API within AAO templates of d = 10 nm (and d = 120 nm), there is no well-resolved interfacial layer formed upon fast cooling. The applied "quenching" thermal protocol might result in a reduced surface interaction of molecules near the interface, and likely decreases the surface coverage as they weaker interact with pore walls with respect to the ones adsorbed upon slow cooling. Therefore, the systems are characterized by a rather bulk-like behavior. Note that no difference between the quenched and slowly cooled PRO infiltrated into AAO membranes of d = 120 nm might result from a rather high value of pore diameter and low surface-to-volume ratio. At those conditions, the surface effects cannot be a dominant factor as in case of pores of much lower radius. Thus, even the presence of the strongly adsorbed interfacial layer does not have so great impact on the behavior of confined PRO. Additionally, it should be mentioned that the

https://dx.doi.org/10.1021/acs.jpcc.0c10560
J. Phys. Chem. C 2021, 125, 3901−3912

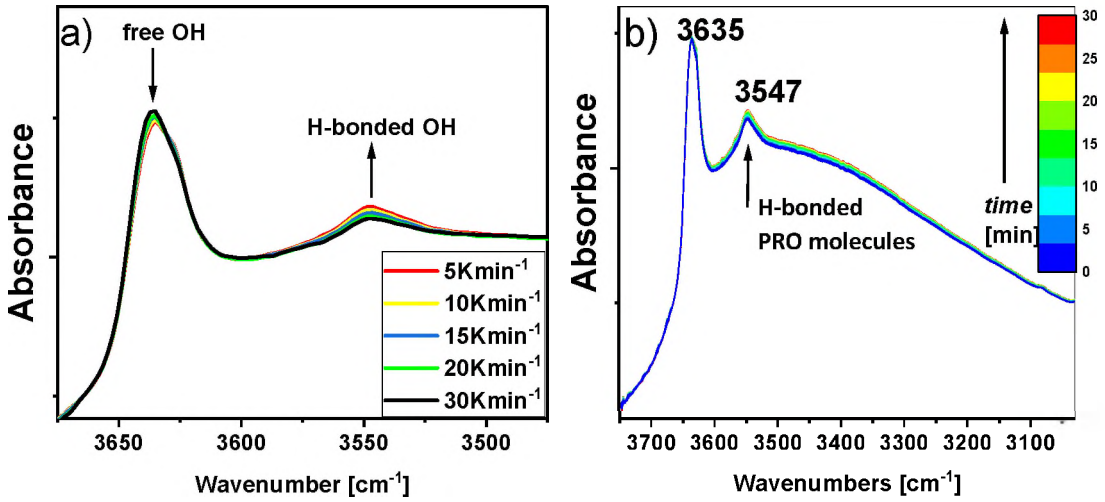

Figure 4. (a) FTIR spectra obtained in the wavenumber region of 3675−3475 cm^{-1} of a confined PRO within AAO membrane (d = 10 nm). The sample was heated to 343 K at a heating rate 10 K min^{-1}, held for 5 min at this temperature and then cooled to T_{anneal} = 308 K at different cooling rates (5, 10, 15, 20, and 30 K min^{-1}). Arrows indicate the direction of band intensity changes with decreasing cooling rate. b) Time-dependent FTIR spectra of a confined PRO within AAO membrane (d = 10 nm) obtained in the wavenumber region of 3800−3020 cm^{-1}. The melted samples were cooled to T_{anneal} = 308 K with a constant cooling rate of 20 K min^{-1}. The arrow indicates the direction of band intensity changes with increasing time.

examined API is characterized by one of the highest values of the dT_g/dp coefficient (=427 K/GPa, which quantifies the sensitivity of this compound to the density changes) reported to date when compared to the other systems described earlier in the literature.[76−79,49] As previously shown by some of us,[75] the higher the value of the dT_g/dp, the greater the deviation of the $T_{g,core}$ from the $T_{g,\ bulk}$ is noted. However, to observe this effect, there must be formed an interfacial layer strongly bonded to the pore walls. Our data clearly indicated that once the sample is cooled very quickly or very slowly below T_g, the confinement-induced effects on the structural dynamics and the T_g depression are either minimal or significant. One can suppose that this experimental finding can be assigned to the adsorption of the API to the pore walls or a formation of H bonds between host and guest materials, which is a time-dependent phenomenon. Contrary to the quenched sample, in the case of slowly cooled systems, there is enough time for API to form a strongly bonded interfacial layer, whose freezing out induces density or free volume fluctuations. As a consequence, a clear deviation in molecular dynamics of the core fraction from the bulk-like behavior and significant depression of the glass transition temperature are detected.

To get a deeper understanding of this phenomenon and verify a hypothesis discussed above, we performed further FTIR measurements. Figure S7 shows FTIR spectra of the crystalline and glassy PRO and the API confined within the AAO membrane in the 3800−2700 cm^{-1} frequency range. In this spectral region, narrow peaks between 3030 and 2830 cm^{-1} are associated with the CH groups' stretching vibrations, while the intense band above 3630 cm^{-1} corresponds to the stretching vibrations of the non-H-bonded "free" hydroxyl groups. The assignment of the low-frequency bands in the IR spectrum of PRO was presented in our earlier work and is not the purpose of this paper.[49] Herein, we focus only on the OH group vibration region, which can provide information about intermolecular, including guest−host, interactions. The existence of exclusively one band about 3630 cm^{-1} indicates that in neat PRO (crystalline and glassy samples), there are no molecular interactions of the O−H···O type as the hydroxyl groups are strongly protected by the steric effect of *tert*-butyl groups. In fact, the literature data for this API show that molecules are held exclusively by weak dispersion forces.[82,83,80] Therefore, it is extremely interesting to study the behavior of such a nonassociating system under spatially limited conditions.

On the other hand, FTIR spectra of confined PRO within AAO membrane revealed as interesting as unexpected results, which are related to the appearance of additional bands that were not detected in the spectra of the bulk system. Interestingly, next to the band of "free" OH groups, a new peak at 3547 cm^{-1} is visible (Figure S6). To explore the nature of this new vibration, we refer to our previous work devoted to PRO glass recovered from the high-pressure experiments.[49] In the case of the compressed PRO, the appearance of the band at 3541 cm^{-1} was assigned to the formation of very weak intermolecular O−H···S hydrogen bonds. It is worthwhile to stress that additional density functional theory (DFT) computations supported such an interpretation. Hence, a close agreement between band positions (3547 and 3541 cm^{-1}) suggests the formation of similar kind weak O−H···S H-bonding interactions in pores. Therefore, quite unexpectedly, in contrast to the literature data showing the suppression of specific interactions for the spatially restricted samples, the infiltration of API into porous alumina templates triggers the self-association process. However, at the same time, it is worth pointing out that we are unable to exclude, whether the interactions of PRO molecules with the membrane surface contribute to this new peak as well. At this point, it should be noted that FTIR spectra of the confined PRO are also distorted by the additional contribution of the stretching vibrations of the OH groups derived from the AAO pore surface; i.e., the maximum of the OH band appears at 3460 cm^{-1} (Figure S8). Hence, the presence of this parasitic band makes the whole analysis and interpretation more difficult.

To verify whether the additional guest−host interactions exist in the studied system, cooling rate and time-dependent IR investigations were performed. Note that the confined PRO was cooled with different cooling rates (5−30 K/min) from T

https://dx.doi.org/10.1021/acs.jpcc.0c10560
J. Phys. Chem. C 2021, 125, 3901−3912

= 343 K prior to measurements at T = 308 K started. Interestingly, the spectra of the confined API showed that the intensity of the IR absorption bands located at 3635 and 3547 cm^{-1}, respectively, decrease and increase as the cooling rate is lowered (see Figure 4a). Assuming that the number of self-assembled H-bonded molecules of API is barely temperature and time-dependent, one can suppose that this effect is related to the change in population of the API adsorbed via H-bonds to the pore walls. Consequently, the slower reduction of temperature, the greater the number of PRO molecules interacting with the alumina surface. Moreover, the band intensity at 3547 cm^{-1} also increases over time, indicating an increasing degree of guest−host interactions due to annealing of the sample previously cooled from T = 343 K with 20 K/min cooling rate (see Figure 4b). Therefore, the observed spectral effects imply the existence of additional processes taking place at the interface, leading to the formation of specific H-bond type interactions of PRO molecules with the surface of the pore walls. This finding confirms that most likely, aside from the O−H···S H association of API molecules, interfacial H-bond type interactions of PRO and alumina matrix also contribute to the additional vibration detected at 3547 cm^{-1}. Furthermore, results obtained from FTIR investigations strongly support the hypothesis that the peculiar behavior of structural dynamics of confined API prepared via two different ways is strongly connected to the time-dependent adsorption and formation of the interfacial H-bonded layer. Once the layer is formed and more strongly adsorbed to the pore walls, the surface effects become magnified. Therefore, the selection of a system with so high dT_g/dp allowed us to prove that not ony the pressure coefficient of the glass transition temperature itself but also properties of interfacial layer underlie the response of the core fraction of molecules confined in porous templates.

Finally, as the last point of our investigation, we probed the physical stability of PRO under confinement. One can recall that controlling the crystallization process by the appropriate parameters of nanoporous host matrices allows developing novel drug carrier systems, which successfully stabilize APIs.[19,41,43,81] Moreover, interestingly, the application of constraining medium also enables to obtain new crystalline (polymorphic) forms of various compounds (including APIs), which are often characterized by different physicochemical properties.[19,41,43] As was clearly shown above, PRO infiltrated into AAO templates of the following pore size, d ∼ 10−160 nm, is amorphous and does not tend to crystallize on the experimental time scale. Thus, to probe the eventual crystallization of the confined API, it was stored for 50 days. After that time, we performed successive DSC and XRD measurements.

The recorded DSC thermograms of the recrystallized both bulk and confined PRO are presented in Figure 3b (the data for bulk API were taken from ref 49). Note that in the case of API infiltrated in AAO templates of d = 10 nm, it remains amorphous even after 50 days; hence, only the data for d > 40 nm are presented. Interestingly, for bulk PRO, one endothermic process, related to melting at T_m = 400 K, can be observed, see Figure 3b. On the other hand, for the confined samples, two melting peaks of significantly different enthalpies, ΔH_m, can be distinguished independently from the applied pore diameter. As illustrated, both peaks shift toward lower temperature with decreasing d when compared to the bulk, see Figure 3b. One can suppose that the presence of two melting points for the infiltrated PRO might be a result of two scenarios, either the crystallization of two various fractions of molecules (interfacial and core) or the existence of two different polymorphs of PRO. Note that previous studies of bulk PRO revealed the presence of two polymorphic forms characterized by different T_m. The stable form I is characterized by a higher melting temperature. $T_{m,I}$ ∼ 398 K, whereas the second unstable form II has a melting point at $T_{m,II}$ ∼ 389 K.[82,83]

To determine the origin of the observed melting peaks in the recorded DSC thermograms, we carried out additional XRD measurements. The diffraction pattern of bulk crystalline PRO exhibits the presence of two polymorphic forms in the sample; see Figure 5a. The greater part of the bulk PRO is composed of

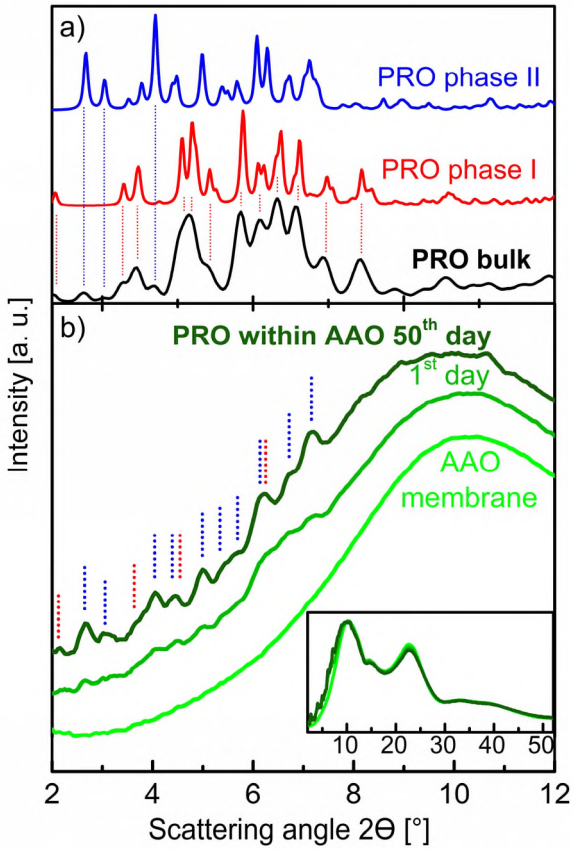

Figure 5. Comparison of X-ray diffraction patterns of bulk PRO sample together with pure references of I and II polymorphic forms (a) and PRO confined into AAO template (d = 80 nm) just after 1 and 50 days of sample storage together with the data for neat AAO membrane (b).

the polymorph I, identified as a monoclinic system with $P2_1/c$ space group symmetry and a ≈ 16.9 Å, b ≈ 10.5 Å, c ≈ 19.0 Å, α ≈ 90°, β ≈ 113.7°, and γ ≈ 90°, according to the Crystallography Open Database (CCDC code: 1172913).[82] The small admixture of polymorph II, which crystallizes in monoclinic system with $P2_1/n$ space group and a ≈ 11.2 Å, b ≈ 16.0 Å, c ≈ 18.8 Å, α ≈ 90°, β ≈ 104.0°, and γ ≈ 90° (CCDC code: 1172912), might also be recognized in the bulk sample based on the positions of the Bragg peaks (marked with blue lines). This observation is in line with earlier reports for bulk PRO,[82] which revealed different conformations in the two polymorphs, where in form II, the C−S−C−S−C chain is

https://dx.doi.org/10.1021/acs.jpcc.0c10560
J. Phys. Chem. C 2021, 125, 3901−3912

extended, and the molecular symmetry approximates C_{2v}. On the other hand, in the case of form I, two S−C−S−C torsion angles are roughly 80° and 165°. As shown, the less symmetrical conformer of polymorph I is more stable than the polymorph II (difference around ∼26 kJ mol^{-1}). The XRD pattern for the sample of PRO confined in AAO pores with d = 80 nm just after 2 and 50 days of storage is presented in Figure 5b. In the case of the sample stored for 1 day, only broad low-intense peaks might be distinguished from the diffraction pattern of the amorphous AAO membrane. However, their positions correspond directly to sharper peaks seen for the sample after 50 days of storage. It means that, during this time, the crystallization of PRO progresses. The confined material is also composed of two polymorphic forms: I and II, as evidenced by the positions of the observed Bragg peaks. However, it should be mentioned that in contrast to the bulk form, PRO infiltrated into AAO is composed of mainly polymorph II and a smaller amount of polymorph I. This means that the observed multiple melting points of PRO under confinement detected by DSC measurements actually originate from the crystallization of various polymorphic forms. Moreover, it should be mentioned that the differences in the melting intensities also indicate that, surprisingly, the less stable form II (with higher intensity) is more favored under confinement in contrast to the bulk sample.

As we confirmed that the observed two melting temperatures are related to the various polymorphic forms of PRO, we decided to calculate the surface energy between crystal and liquid, σ_{cl}, of PRO, that is a key quantity to evaluate the critical radius of nucleation, r_c, as well as to predict the energetic barrier for the nucleation process. It should be highlighted that σ_{cl} cannot be determined experimentally for bulk materials;[34,84] however, accordingly to the Gibbs−Thomson (GT) equation,[39] it might be easily calculated for confined samples:

$$\Delta T_m = (T_m - T_m(d)) = \frac{4\sigma_{cl}T_m}{d\Delta H_m\rho_c} \quad (2)$$

where $T_m(d)$ is a melting temperature of crystals formed in pores of different pore diameters, ρ_c is a crystal density, and ΔH_m is a melting enthalpy. The following parameters, ρ_c, σ_{cl}, and ΔH_m, refer to bulk values. Note that according to the literature, form I is characterized by ρ_c = 1.1 ± 0.1 g/cm^3 and ΔH_m = 64 J/g, whereas form II is characterized by ρ_c= 1.049 g/cm^3 and ΔH_m = 68 J/g.[80,82] It should be mentioned that both melting points of the examined confined systems decrease with a reduction of pore size, as postulated by the GT relation. Consequently, the surface energy of PRO, calculated using the values of $T_{m,I}$ and $T_{m,II}$, respectively, is equal to σ_{cl} ∼ 23 mJ/m^2 and σ_{cl} ∼ 26.5 mJ/m^2. It should be highlighted that, for these systems, the surface energy, σ_{cl}, is quite similar to those calculated for other low molecular weight systems.[85−87]

Subsequently, we also calculated the critical radius of nucleation, r_c, of both forms:[34,84]

$$r_{c,i} = \frac{2\sigma_{cl,i}T_{m,i}}{\Delta H_{m,i}\rho_C\Delta T_i} \quad (3)$$

where $T_{m,i}$ is a melting point of bulk material ($T_{m,I}$ = 400 K and $T_{m,II}$ = 389 K, respectively). Afterward, we determined the critical size of nuclei for different pore sizes as a function of reduced temperature, $\Delta T_i = T_{m,i} - T$, see Figure S9. Note that r_c was calculated with the use of both observed T_ms. The obtained size of nuclei decreases with increasing undercooling, reaching approximately r_c ∼ 3 nm at RT for both polymorphic forms. This relatively low value of r_c means that PRO should be able to crystallize even inside the smallest pore size applied in this study, d = 10 nm. However, it is not the case. Interestingly, similar behavior (r_c < d) has been reported for fenofibrate confined within controlled pore glass (CPG of d < 20 nm), where the crystallization of this pharmaceutical was completely suppressed.[88] One can suppose that the inhibition of crystallization of PRO infiltrated into AAO templates of d = 10 nm might be related to the enhanced surface H-bonded type interactions between the API and pore walls as well as the self-association process, completely absent for the bulk substance but induced in the confined PRO.

4. CONCLUSIONS

In conclusion, the molecular dynamics of PRO confined into AAO matrices of various pore diameters was strongly dependent on the applied thermal pathway. Although for all confined samples, we observed a "typical" deviation of $\tau_\alpha(T)$-dependences from the bulk-like behavior, these dependencies in the case of the quenched systems differed significantly from those measured on slow cooling. As illustrated, the slowly cooled materials are characterized by enhanced molecular dynamics when approaching T_g. To the best of our knowledge, the effect observed herein (as well as enormous variations between both thermal histories) is reported for the first time for the liquid infiltrated into pores. We assume that the differences between the dynamics of confined PRO measured on slow cooling and heating might be strictly correlated with surface effects, especially the density perturbation within the interfacial layer as well as the adsorption−desorption effects occurring near the interface. The impact of these processes affecting the density packing fluctuations is magnified in PRO since it is characterized by the extremely high value of the pressure coefficient of the glass transition temperature (dT_g/dp). Additionally, as concluded from FTIR studies, the pores induce the association process between PRO molecules. The H-bonded interfacial layer, whose properties depend on the time of annealing and cooling rate, is formed. We assumed that the (re)formed H-bonding structure of PRO influences its structural dynamics and contributes to the peculiar behavior of confined API. Thus, a selection of a system with so high a dT_g/dp allowed us to prove that not only this parameter itself but also properties of interfacial layer underlie the response of the core fraction of molecules confined in porous templates. Moreover, it was found that the applied nanometrical geometrical restriction reduces the tendency to crystallization of amorphous PRO infiltrated into AAO templates when compared to the bulk. Simultaneously, it should be mentioned that the recrystallized API revealed the presence of two melting temperatures under confinement. XRD measurements confirmed that they correspond to the two polymorphic forms, stable form I (dominating in bulk) and unstable form II (prevailing under confinement). We believe that the presented results shed new light on the mutual correlation between the surface effects and the sensitivity to the density fluctuation, and they impact on the behavior of soft matter confined in porous templates.

■ ASSOCIATED CONTENT

Supporting Information

The Supporting Information is available free of charge at https://pubs.acs.org/doi/10.1021/acs.jpcc.0c10560.

https://dx.doi.org/10.1021/acs.jpcc.0c10560
J. Phys. Chem. C 2021, 125, 3901−3912

Additional figures, including dielectric spectra collected for PRO within pore diameters d = 120 nm and d = 80 nm; relaxation maps for PRO infiltrated into AAO membranes with different pore diameters; DSC thermograms; derivative representation of the heat flow for confined PRO; FTIR spectra; and estimation of the radius of critical nuclei, r_c (PDF)

AUTHOR INFORMATION

Corresponding Authors

Agnieszka Talik − *Institute of Physics, University of Silesia in Katowice, 41-500 Chorzow, Poland; Silesian Center of Education and Interdisciplinary Research, University of Silesia in Katowice, 41-500 Chorzow, Poland;* orcid.org/0000-0001-7940-6967; Email: agnieszka.talik@smcebi.edu.pl

Magdalena Tarnacka − *Institute of Physics, University of Silesia in Katowice, 41-500 Chorzow, Poland; Silesian Center of Education and Interdisciplinary Research, University of Silesia in Katowice, 41-500 Chorzow, Poland;* orcid.org/0000-0002-9444-3114; Email: magdalena.tarnacka@smcebi.edu.pl

Authors

Aldona Minecka − *Department of Pharmacognosy and Phytochemistry, Faculty of Pharmaceutical Sciences in Sosnowiec, Medical University of Silesia in Katowice, 41-200 Sosnowiec, Poland;* orcid.org/0000-0001-5603-032X

Barbara Hachuła − *Institute of Chemistry and Silesian Center of Education and Interdisciplinary Research, University of Silesia in Katowice, 40-006 Katowice, Poland*

Joanna Grelska − *Institute of Physics, University of Silesia in Katowice, 41-500 Chorzow, Poland; Silesian Center of Education and Interdisciplinary Research, University of Silesia in Katowice, 41-500 Chorzow, Poland*

Karolina Jurkiewicz − *Institute of Physics, University of Silesia in Katowice, 41-500 Chorzow, Poland; Silesian Center of Education and Interdisciplinary Research, University of Silesia in Katowice, 41-500 Chorzow, Poland;* orcid.org/0000-0002-4289-7827

Kamil Kaminski − *Institute of Physics, University of Silesia in Katowice, 41-500 Chorzow, Poland; Silesian Center of Education and Interdisciplinary Research, University of Silesia in Katowice, 41-500 Chorzow, Poland;* orcid.org/0000-0002-5871-0203

Marian Paluch − *Institute of Physics, University of Silesia in Katowice, 41-500 Chorzow, Poland; Silesian Center of Education and Interdisciplinary Research, University of Silesia in Katowice, 41-500 Chorzow, Poland*

Ewa Kaminska − *Department of Pharmacognosy and Phytochemistry, Faculty of Pharmaceutical Sciences in Sosnowiec, Medical University of Silesia in Katowice, 41-200 Sosnowiec, Poland;* orcid.org/0000-0001-9725-8654

Complete contact information is available at: https://pubs.acs.org/10.1021/acs.jpcc.0c10560

Notes

The authors declare no competing financial interest.

ACKNOWLEDGMENTS

M.T., K.K. and M.P. are thankful for financial support from the Polish National Science Centre within the OPUS project (Dec. No. 2019/33/B/ST3/00500). E.K. is grateful for the financial support from the National Science Centre within the framework of the Sonata BIS project (Dec. No. 2016/22/E/NZ7/00266). K.J. is thankful for the financial support from the Foundation for Polish Science within the START program. A.M. is grateful for financial support from the Medical University of Silesia within Research for Young Scientists (Contract No. KNW-2-O-34/D/9/N).

REFERENCES

(1) Kalepu, S.; Nekkanti, V. Insoluble drug delivery strategies: Review of recent advances and business prospects. *Acta Pharm. Sin. B* **2015**, *5*, 442−453.

(2) Hillery, A. M.; Park, K. *Drug delivery: Fundamentals and applications*, 2nd ed.; CRC Press: 2016.

(3) Gupta, D.; Bhatia, D.; Dave, V.; Sutariya, V.; Varghese Gupta, S. Salts of therapeutic agents: Chemical, physicochemical, and biological considerations. *Molecules* **2018**, *23*, 1719.

(4) Elder, D. P.; Delaney, E.; Teasdale, A.; Eyley, S.; Reif, V. D.; Jacq, K.; Facchine, K. L.; Oestrich, R. S.; Sandra, P.; David, F. The utility of sulfonate salts in drug development. *J. Pharm. Sci.* **2010**, *99*, 2948−2961.

(5) Huang, L. F.; Tong, W. Q. Impact of solid state properties on developability assessment of drug candidates. *Adv. Drug Delivery Rev.* **2004**, *56*, 321−334.

(6) Olusanmi, D.; Jayawickrama, D.; Bu, D.; McGeorge, G.; Sailes, H.; Kelleher, J.; Gamble, J. F.; Shah, U. V.; Tobyn, M. A control strategy for bioavailability enhancement by size reduction: effect of micronization conditions on the bulk, surface and blending characteristics of an active pharmaceutical ingredient. *Powder Technol.* **2014**, *258*, 222−233.

(7) D, S.; Muthudoss, P.; Khullar, P.; A, R. V. Micronization and agglomeration: Understanding the impact of API particle properties on dissolution and permeability using solid state and biopharmaceutical "Toolbox. *J. Pharm. Innov.* **2020**, DOI: 10.1007/s12247-019-09424-1.

(8) Karagianni, A.; Malamatari, M.; Kachrimanis, K. Pharmaceutical cocrystals: New solid phase modification approaches for the formulation of APIs. *Pharmaceutics* **2018**, *10*, 18.

(9) Dai, X.-L.; Chen, J.-M.; Lu, T.-B. Pharmaceutical cocrystallization: an effective approach to modulate the physicochemical properties of solid-state drugs. *CrystEngComm* **2018**, *20*, 5292−5316.

(10) Saito, M.; Ugajin, T.; Nozawa, Y.; Sadzuka, Y.; Miyagishima, A.; Sonobe, T. Preparation and dissolution characteristics of griseofulvin solid dispersions with saccharides. *Int. J. Pharm.* **2002**, *249*, 71−79.

(11) Kawakami, K. *Recent progress in solid dispersion technology. Pharmaceutics*; MDPI: 2019.

(12) Zhou, D.; Zhang, G. G. Z.; Law, D.; Grant, D.W. J.; Schmitt, E. A. Physical stability of amorphous pharmaceuticals: importance of configurational thermodynamic quantities and molecular mobility. *J. Pharm. Sci.* **2002**, *91*, 1863−1872.

(13) Hancock, B. C.; Zografi, G. Characteristics and significance of the amorphous state in pharmaceutical systems. *J. Pharm. Sci.* **1997**, *86*, 1−12.

(14) Wyttenbach, N.; Kuentz, M. Glass-forming ability of compounds in marketed amorphous drug products. *Eur. J. Pharm. Biopharm.* **2017**, *112*, 204−208.

(15) Yu, L. Amorphous pharmaceutical solids: preparation, characterization and stabilization. *Adv. Drug Delivery Rev.* **2001**, *48*, 27−42.

(16) Grzybowska, K.; Paluch, M.; Włodarczyk, P.; Grzybowski, A.; Kaminski, K.; Hawelek, L.; Zakowiecki, D.; Kasprzycka, A.; Jankowska-Sumara, I. Enhancement of amorphous celecoxib stability by mixing it with octaacetylmaltose: The molecular dynamics study. *Mol. Pharmaceutics* **2012**, *9*, 894−904.

(17) Schammé, B.; Couvrat, N.; Tognetti, V.; Delbreilh, L.; Dupray, V.; Dargent, E.; Coquerel, G. Investigation of drug-excipient

interactions in biclotymol amorphous solid dispersions. *Mol. Pharmaceutics* **2018**, *15*, 1112−1125.
(18) Kaminska, E.; Adrjanowicz, K.; Tarnacka, M.; Kolodziejczyk, K.; Dulski, M.; Mapesa, E. U.; Zakowiecki, D.; Hawełek, Ł.; Kaczmarczyk-Sedlak, I.; Kaminski, K. Impact of inter- and intramolecular interactions on the physical stability of indomethacin dispersed in acetylated saccharides. *Mol. Pharmaceutics* **2014**, *11*, 2935−2947.
(19) Madejczyk, O.; Kaminska, E.; Tarnacka, M.; Dulski, M.; Jurkiewicz, K.; Kaminski, K.; Paluch, M. Studying the crystallization of various polymorphic forms of nifedipine from binary mixtures with the use of different experimental techniques. *Mol. Pharmaceutics* **2017**, *14*, 2116−2125.
(20) Minecka, A.; Kamińska, E.; Tarnacka, M.; Jurkiewicz, M.; Talik, A.; Wolnica, K.; Dulski, M.; Kasprzycka, A.; Spychalska, P.; Garbacz, G.; et al. Does the molecular mobility and flexibility of the saccharide ring affect the glass-forming ability of naproxen in binary mixtures? *Eur. J. Pharm. Sci.* **2020**, *141*, 105091.
(21) Taylor, L. S.; Zografi, G. Spectroscopic characterization of interactions between PVP and indomethacin in amorphous molecular dispersions. *Pharm. Res.* **1997**, *14*, 1691−1698.
(22) Wegiel, L. A.; Mauer, L. I.; Edgar, K. J.; Taylor, L. S. Crystallization of amorphous solid dispersions of resveratrol during preparation and storage—impact of different polymers. *J. Pharm. Sci.* **2013**, *102*, 171−184.
(23) Khodaverdi, K.; Khalili, N.; Zangiabadi, F.; Homayouni, A. Preparation, characterization and stability studies of glassy solid dispersions of indomethacin using pvp and isomalt as carriers. *Iran J. Basic Med. Sci.* **2012**, *15*, 820−832.
(24) Sun, Y.; Tao, J.; Zhang, G. G. Z.; Yu, L. Solubilities of crystalline drugs in polymers: An improved analytical method and comparison of solubilities of indomethacin and nifedipine in PVP, PVP/VA, and PVAc. *J. Pharm. Sci.* **2010**, *99*, 4023−4031.
(25) Zhao, M.; Barker, S. A.; Belton, P. S.; McGregor, C.; Craig, D. Q. M. Development of fully amorphous dispersions of a low Tg drug via co-spray drying with hydrophilic polymers. *Eur. J. Pharm. Biopharm.* **2012**, *82*, 572−579.
(26) Löbmann, K.; Grohganz, H.; Laitinen, R.; Strachan, C.; Rades, T. Amino acids as co-amorphous stabilizers for poorly water soluble drugs − Part 1: Preparation, stability and dissolution enhancement. *Eur. J. Pharm. Biopharm.* **2013**, *85*, 873−881.
(27) Löbmann, K.; Laitinen, R.; Strachan, C.; Rades, T.; Grohganz, H. Amino acids as co-amorphous stabilizers for poorly water-soluble drugs − Part 2: Molecular interactions. *Eur. J. Pharm. Biopharm.* **2013**, *85*, 882−888.
(28) Jensen, K. T.; Löbmann, K.; Rades, T.; Grohganz, H. Improving co-amorphous drug formulations by the addition of the highly water soluble amino acid, proline. *Pharmaceutics* **2014**, *6*, 416−435.
(29) Cordeiro, T.; Castiñeira, C.; Mendes, D.; Danède, F.; Sotomayor, J.; Fonseca, I. M.; Gomes da Silva, M.; Paiva, A.; Barreiros, S.; Cardoso, M. M.; et al. Stabilizing unstable amorphous menthol through inclusion in mesoporous silica hosts. *Mol. Pharmaceutics* **2017**, *14*, 3164−3177.
(30) Cordeiro, T.; Santos, A. F. M.; Nunes, G.; Cunha, G.; Sotomayor, J. C.; Fonseca, I. M.; Danède, F.; Dias, C. J.; Cardoso, M. M.; Correia, N. T.; et al. Accessing the physical state and molecular mobility of naproxen confined to nanoporous silica matrixes. *J. Phys. Chem. C* **2016**, *120*, 14390−14401.
(31) Bras, A. R.; Merino, E. G.; Neves, P. D.; Fonseca, I. M.; Dionísio, M. A.; Schonhals, A.; Correia, N. T. Amorphous ibuprofen confined in nanostructured silica materials: A dynamical approach. *J. Phys. Chem. C* **2011**, *115*, 4616−4623.
(32) Braś, A. R.; Fonseca, I. M.; Dionísio, M.; Schönhals, A.; Affouard, F.; Correia, N. T. Influence of nanoscale confinement on the molecular mobility of ibuprofen. *J. Phys. Chem. C* **2014**, *118*, 13857−13868.
(33) Knapik, J.; Wojnarowska, Z.; Grzybowska, K.; Jurkiewicz, K.; Stankiewicz, A.; Paluch, M. Stabilization of the amorphous ezetimibe drug by confining its dimension. *Mol. Pharmaceutics* **2016**, *13*, 1308−1316.
(34) Szklarz, G.; Adrjanowicz, K.; Tarnacka, M.; Pionteck, J.; Paluch, M. Confinement-induced changes in the glassy dynamics and crystallization behavior of supercooled fenofibrate. *J. Phys. Chem. C* **2018**, *122*, 1384−1395.
(35) Minecka, A.; Kaminska, E.; Tarnacka, M.; Grudzka-Flak, I.; Bartoszek, M.; Wolnica, K.; Dulski, M.; Kaminski, K.; Paluch, M. The impact of intermolecular interactions, dimeric structures on the glass forming ability of naproxen and a series of its derivatives. *Mol. Pharmaceutics* **2018**, *15*, 4764−4776.
(36) Suzuki, Y.; Duran, H.; Steinhart, M.; Kappl, M.; Butt, H.-J.; Floudas, G. Homogeneous nucleation of predominantly cubic ice confined in nanoporous alumina. *Nano Lett.* **2015**, *15*, 1987−1992.
(37) Suzuki, Y.; Steinhart, M.; Graf, R.; Butt, H.-J.; Floudas, G. Dynamics of ice/water confined in nanoporous alumina. *J. Phys. Chem. B* **2015**, *119*, 14814−14820.
(38) Yao, Y.; Fella, V.; Huang, W.; Zhang, K. A. I.; Landfester, K.; Butt, H.-J.; Vogel, M.; Floudas, G. Crystallization and dynamics of water confined in model mesoporous silica particles: Two ice nuclei and two fractions of water. *Langmuir* **2019**, *35*, 5890−5901.
(39) Defay, R.; Prigogine, I.; Bellemans, A.; Everett, D. H. *Surface tension and adsorption*; Wiley: New York, 1966.
(40) Jackson, C. L.; Mckenna, G. B. The melting behavior of organic materials confined in porous solids. *J. Chem. Phys.* **1990**, *93*, 9002−9011.
(41) Bishara, H.; Berger, S. Polymorphism and piezoelectricity of glycine nano-crystals grown inside alumina nano-pores. *J. Mater. Sci.* **2019**, *54*, 4619−4625.
(42) Rengarajan, G. T.; Enke, D.; Beiner, M. Crystallization behavior of acetaminophen in nanopores. *Open Phys. Chem. J.* **2007**, *1*, 18−24.
(43) Kołodziejczyk, K.; Tarnacka, M.; Kaminska, E.; Dulski, M.; Kaminski, K.; Paluch, M. The crystallization's kinetic under confinement. Manipulation of the crystalline form of salol by varying pore diameter. *Cryst. Growth Des.* **2016**, *16*, 1218−1227.
(44) Adrjanowicz, K.; Kolodziejczyk, K.; Kipnusu, W. K.; Tarnacka, M.; Mapesa, E. U.; Kaminska, E.; Pawlus, S.; Kaminski, K.; Paluch, M. Decoupling between the interfacial and core molecular dynamics of salol in 2D confinement. *J. Phys. Chem. C* **2015**, *119*, 14366−14374.
(45) Tarnacka, M.; Kipnusu, W. K.; Kaminska, E.; Pawlus, S.; Kaminski, K.; Paluch, M. The peculiar behavior of the molecular dynamics of a glass-forming liquid confined in native porous materials − the role of negative pressure. *Phys. Chem. Chem. Phys.* **2016**, *18*, 23709−23714.
(46) Kipnusu, W. K.; Elmahdy, M. M.; Elsayed, M.; Krause-Rehberg, R.; Kremer, F. Counterbalance between surface and confinement effects as studied for amino-terminated poly(propylene glycol) constraint in silica nanopores. *Macromolecules* **2019**, *52*, 1864−1873.
(47) Morineau, D.; Xia, Y.; Alba-Simionesco, C. Finite-size and surface effects on the glass transition of liquid toluene confined in cylindrical mesopores. *J. Chem. Phys.* **2002**, *117*, 8966−8972.
(48) Lau, M.; Giri, K.; Garcia-Bennett, A. E. Antioxidant properties of probucol released from mesoporous silica. *Eur. J. Pharm. Sci.* **2019**, *138*, 105038.
(49) Kamińska, E.; Minecka, A.; Tarnacka, M.; Kamiński, K.; Paluch, M. Breakdown of the isochronal structural (α) and secondary (JG β) exact superpositioning in probucol - A low molecular weight pharmaceutical. *J. Mol. Liq.* **2020**, *299*, 112169.
(50) https://www.inredox.com.
(51) Iacob, C.; Sangoro, J. R.; Papadopoulos, P.; Schubert, T.; Naumov, S.; Valiullin, R.; Karger, J.; Kremer, F. Charge transport and diffusion of ionic liquids in nanoporous silica membranes. *Phys. Chem. Chem. Phys.* **2010**, *12*, 13798.
(52) Kipnusu, W. K.; Kossack, W.; Iacob, C.; Jasiurkowska, M.; Rume Sangoro, J.; Kremer, F. Molecular order and dynamics of tris(2ethylhexyl)phosphate confined in uni-directional nanopores. *Z. Phys. Chem.* **2012**, *226*, 797−805.
(53) Alexandris, S.; Papadopoulos, P.; Sakellariou, G.; Steinhart, M.; Butt, H.-J.; Floudas, G. Interfacial energy and glass temperature of

https://dx.doi.org/10.1021/acs.jpcc.0c10560
J. Phys. Chem. C 2021, 125, 3901−3912

polymers confined to nanoporous alumina. *Macromolecules* **2016**, *49*, 7400−7414.
(54) Tarnacka, M.; Dulski, M.; Geppert-Rybczyńska, M.; Talik, A.; Kaminska, E.; Kaminski, K.; Paluch, M. Variation in the molecular dynamics of DGEBA confined within AAO templates above and below the glass transition temperature. *J. Phys. Chem. C* **2018**, *122*, 28033−28044.
(55) Kremer, F. *Dynamics in geometrical confinement*; Springer: Switzerland, 2014.
(56) Alexandris, S.; Sakellariou, G.; Steinhart, M.; Floudas, G. Dynamics of unentangled cis-1,4-polyisoprene confined to nanoporous alumina. *Macromolecules* **2014**, *47*, 3895−3900.
(57) Tarnacka, M.; Kaminski, K.; Mapesa, E. U.; Kaminska, E.; Paluch, M. Studies on the temperature and time induced variation in the segmental and chain dynamics in poly(propylene glycol) confined at the nanoscale. *Macromolecules* **2016**, *49*, 6678−6686.
(58) Huwe, A.; Arndt, M.; Kremer, F.; Haggenmüller, C.; Behrens, P. Dielectric investigations of the molecular dynamics of propanediol in mesoporous silica materials. *J. Chem. Phys.* **1997**, *107*, 9699−9701.
(59) Adrjanowicz, K.; Kaminski, K.; Koperwas, K.; Paluch, M. Negative pressure vitrification of the isochorically confined liquid in nanopores. *Phys. Rev. Lett.* **2015**, *115*, 265702.
(60) Park, J.-Y.; McKenna, G. B. Size and confinement effects on the glass transition behavior of Polystyrene/O-terphenyl polymer solutions. *Phys. Rev. B: Condens. Matter Mater. Phys.* **2000**, *61*, 6667−6676.
(61) Arndt, M.; Stannarius, R.; Gorbatschow, W.; Kremer, F. Dielectric investigations of the dynamic glass transition in nanopores. *Phys. Rev. E: Stat. Phys., Plasmas, Fluids, Relat. Interdiscip. Top.* **1996**, *54*, 5377−5390.
(62) Tarnacka, M.; Kaminska, E.; Kaminski, K.; Roland, C. M.; Paluch, M. Interplay between core and interfacial mobility and its impact on the measured glass transition: Dielectric and calorimetric studies. *J. Phys. Chem. C* **2016**, *120*, 7373−7380.
(63) Talik, A.; Tarnacka, M.; Geppert-Rybczyńska, M.; Hachuła, B.; Kaminski, K.; Paluch, M. The Impact of confinement on the dynamics and H-bonding pattern in low-molecular weight poly(propylene glycols). *J. Phys. Chem. C* **2020**, *124*, 17607−17621.
(64) Adrjanowicz, K.; Paluch, M. Discharge of the nanopore confinement effect on the glass transition dynamics via viscous flow. *Phys. Rev. Lett.* **2019**, *122*, 176101.
(65) Havriliak, S.; Negami, S. A complex plane representation of dielectric and mechanical relaxation processes in some polymers. *Polymer* **1967**, *8*, 161−210.
(66) Kremer, F.; Schönhals, A. *Broadband dielectric spectroscopy*; Springer: Berlin, 2003.
(67) Arndt, M.; Stannarius, R.; Groothues, H.; Hempel, E.; Kremer, F. Length scale of cooperativity in the dynamic glass transition. *Phys. Rev. Lett.* **1997**, *79*, 2077−2080.
(68) Hong, L.; Gujrati, P. D.; Novikov, V. N.; Sokolov, A. P. Molecular cooperativity in the dynamics of glass-forming systems: A new insight. *J. Chem. Phys.* **2009**, *131*, 194511.
(69) Fischer, J. K. H; Sippel, P.; Denysenko, D.; Lunkenheimer, P.; Volkmer, D.; Loidl, A. Metal-organic frameworks as host materials of confined supercooled liquids. *J. Chem. Phys.* **2015**, *143*, 154505.
(70) Uhl, M.; Fischer, J. K. H.; Sippel, P.; Bunzen, H.; Lunkenheimer, P.; Volkmer, D.; Loidl, A. Glycerol confined in zeolitic imidazolate frameworks: The temperature-dependent cooperativity length scale of glassy freezing. *J. Chem. Phys.* **2019**, *150*, 024504.
(71) Winkler, R.; Tu, W.; Laskowski, Ł.; Adrjanowicz, K. Effect of surface chemistry on the glass-transition dynamics of poly(phenyl methyl siloxane) confined in alumina nanopores. *Langmuir* **2020**, *36*, 7553−7565.
(72) Li, L.; Chen, J.; Deng, W.; Zhang, C.; Sha, Y.; Cheng, Z.; Xue, G.; Zhou, D. Glass transitions of poly(methyl methacrylate) confined in nanopores: Conversion of three- and two-layer models. *J. Phys. Chem. B* **2015**, *119*, 5047−5054.
(73) Casalini, R.; Roland, C. M. Temperature and density effects on the local segmental and global chain dynamics of poly-(oxybutylene). *Macromolecules* **2005**, *38*, 1779−1788.
(74) Kipnusu, W. K.; Elsayed, M.; Kossack, W.; Pawlus, S.; Adrjanowicz, K.; Tress, M.; Mapesa, E. U.; Krause-Rehberg, R.; Kaminski, K.; Kremer, F. Confinement for more space: A larger free volume and enhanced glassy dynamics of 2-ethyl-1-hexanol in nanopores. *J. Phys. Chem. Lett.* **2015**, *6*, 3708−3712.
(75) Talik, A.; Tarnacka, M.; Geppert-Rybczynska, M.; Minecka, A.; Kaminska, E.; Kaminski, K.; Paluch, M. Impact of the interfacial energy and density fluctuations on the shift of the glass-transition temperature of liquids confined in pores. *J. Phys. Chem. C* **2019**, *123*, 5549−5556.
(76) Floudas, G.; Paluch, M.; Grzybowski, A.; Ngai, K. L. *Molecular dynamics of glass-forming systems*; Springer-Verlag, Berlin and Heidelberg, Germany, 2011; Chapter 2.
(77) Kaminska, E.; Tarnacka, M.; Jurkiewicz, K.; Kaminski, K.; Paluch, M. High pressure dielectric studies on the structural and orientational glass. *J. Chem. Phys.* **2016**, *144*, 054503.
(78) Casalini, R.; Roland, C. M. Dielectric α-relaxation and ionic conductivity in propylene glycol and its oligomers measured at elevated pressure. *J. Chem. Phys.* **2003**, *119*, 11951.
(79) Atake, T.; Angell, C. A. Pressure dependence of the glass transition temperature in molecular liquids and plastic crystals. *J. Phys. Chem.* **1979**, *83*, 3218−3223.
(80) Rexrode, R. N.; Orien, J.; King, M. D. Effects of solvent stabilization on pharmaceutical crystallization: Investigating conformational polymorphism of probucol using combined solid-state density functional theory, molecular dynamics, and terahertz spectroscopy. *J. Phys. Chem. A* **2019**, *123*, 6937−6947.
(81) Jiang, Q.; Ward, M. D. Crystallization under nanoscale confinement. *Chem. Soc. Rev.* **2014**, *43*, 2066−2079.
(82) Gerber, J. J.; Caira, M. R.; Lötter, A. P. Structures of two conformational polymorphs of the cholesterol-lowering drug probucol. *J. Crystallogr. Spectrosc. Res.* **1993**, *23*, 863−869.
(83) Kawakami, K.; Ohba, C. Crystallization of probucol from solution and the glassy state. *Int. J. Pharm.* **2017**, *517*, 322−328.
(84) Mullin, J. W. *Crystallization*, 4th ed.; Butterworth-Heinemann: Oxford, 2001.
(85) Alcoutlabi, M.; McKenna, G. B. Effects of confinement on material behaviour at the nanometre size scale. *J. Phys.: Condens. Matter* **2005**, *17*, R461−RS24.
(86) Jackson, C.; McKenna, G. Vitrification and crystallization of organic liquids confined to nanoscale pores. *Chem. Mater.* **1996**, *8*, 2128−2137.
(87) Adrjanowicz, K.; Szklarz, G.; Koperwas, K.; Paluch, M. Comparison of high pressure and nanoscale confinement effects on crystallization of the molecular glass-forming liquid, dimethyl phthalate. *Phys. Chem. Chem. Phys.* **2017**, *19*, 14366−14375.
(88) Dwyer, L. M.; Michaelis, V. K.; O'Mahony, M.; Griffin, R. G.; Myerson, A. S. Confined crystallization of fenofibrate in nanoporous silica. *CrystEngComm* **2015**, *17*, 7922−7929.

https://dx.doi.org/10.1021/acs.jpcc.0c10560
J. Phys. Chem. C 2021, 125, 3901−3912